

# **Robust Surface Hall Effect and Nonlocal Transport in SmB<sub>6</sub>: Indication for an Ideal Topological Insulator**

J. Botimer\*, D.J. Kim\*, S. Thomas\*, T. Grant\*, Z. Fisk and Jing Xia

*Dept. of Physics and Astronomy, University of California, Irvine, California 92697, USA*

(\* These authors contributed equally to this work.)

**A topological insulator (TI) is an unusual quantum state in which the insulating bulk is topologically distinct from vacuum, resulting in a unique metallic surface that is robust against time-reversal invariant perturbations. When placed in a magnetic field, the two-dimensional surface necessarily leads to a surface Hall effect that is independent of sample thickness. Robust nonlocal transport through the highly conductive surface defies Ohm's law and could be extremely useful for energy efficient information processing. These "ideal" behaviors of TI, however, remains elusive in crystals of existing TI (Bi<sub>2</sub>Se<sub>3</sub>, Bi<sub>2</sub>Te<sub>3</sub> and Sb<sub>2</sub>Te<sub>3</sub>) due to impurity caused bulk conduction. We report in large crystals of SmB<sub>6</sub> the surface Hall effects and non-local transport, which are robust against perturbations including mechanical abrasion. The experimental data agree quantitatively with the model of an ideal TI. Using vacuum annealing, we have achieved a surface carrier mobility of 72,000 cm<sup>2</sup>/Vs, highlighting its potential for low-power electronics. Unlike existing weakly interacting TI materials, the strong electron correlation in SmB<sub>6</sub> may give rise to emergent topological quantum phases useful for spintronics and protected quantum computers.**

Recently discovered <sup>1-5</sup> three-dimensional (3D) topological insulators (TI) have generated great excitement since they are beyond the conventional paradigm of broken-symmetries. Strong spin-

orbit coupling in a TI gives rise to a non-trivial and robust conducting surface state surrounding its insulating bulk<sup>4,5</sup>, a novel property not seen in normal insulators and can lead to many novel applications<sup>4,5</sup>. As a result the electronic transport in TI follows unusual electrodynamic laws. The conduction is extremely two-dimensional and causes little dissipation, resulting in large nonlocal voltages that invalidate Ohm's law, reminiscent to those<sup>6,7</sup> found in quantum Hall (QH)<sup>8,9</sup> and quantum spin Hall (QSH)<sup>10,11</sup> states. When placed in a magnetic field, the Hall effect will be highly two-dimensional (2D) and is independent of sample thickness. Since the surface state is protected by time-reversal symmetry, both effects should be robust against non-magnetic perturbations. Although the unique energetics of TI have already been confirmed<sup>4,5</sup> in crystals of Se and Te based TI materials<sup>2-5</sup> by Angle-resolved photoemission spectroscopy (ARPES)<sup>2,3</sup> and STM<sup>12-14</sup>, the above defining and extremely useful transport properties has remained elusive. Even after extensive materials science efforts<sup>15-19</sup>, the bulk of these crystals remain metallic due to impurity conduction, promoting us to search for new types of TI with better material qualities. More importantly, so far most theoretical and experimental efforts have been dedicated to materials with the underlying physics of non-interacting electrons<sup>1,4,5,10</sup>. A big question thus concerns the role of electron interaction and competing orders in new TI materials with strong correlation, from which new types of topological phases are expected to emerge<sup>4,5</sup>.

Meanwhile in the strongly correlated material SmB<sub>6</sub>, many exotic properties<sup>20-22</sup> still defies a satisfactory understanding within the framework of conventional insulators, 40 years<sup>23</sup> after its discovery. SmB<sub>6</sub> is a heavy fermion material, in which highly renormalized f-electrons, hybridized with conduction electrons, form a completely filled band of quasiparticles with an excitation gap  $\Delta$  of about 40 Kelvin. Behaving electronically like an insulator at high

temperatures, at low temperature its resistance mysteriously saturates: a curiosity that is usually attributed to the existence of density of states within the band gap. These “in-gap-states” remind us of the topological surface state of a TI and were indeed experimentally identified in recent ARPES measurements <sup>24</sup>, except it is unclear whether they are located on the surface or are distributed throughout the bulk. Our recent capacitance measurements on high quality SmB<sub>6</sub> crystals revealed intriguing anomalous capacitance effects <sup>25</sup> that could be explained by assuming the in-gap-states exist on the surface. The resemblance between SmB<sub>6</sub> and a TI is echoed by recent theoretical insights <sup>26</sup>: The hybridization and odd parity wavefunction lead to strong spin-orbit coupling in SmB<sub>6</sub> and is proposed to make it a strong TI. In this paper we present evidences of robust surface Hall effect and nonlocal transport in high quality SmB<sub>6</sub> crystals of various geometries and from different growth batches. These results reveal in SmB<sub>6</sub> a perfectly insulating bulk and a protected conducting surface, and highly suggest SmB<sub>6</sub> to be an ideal TI.

Hall effect measurements were carried out in wedge-shaped SmB<sub>6</sub> crystals. As depicted in the inset in Fig. 1(a), the sample is placed in a perpendicular magnetic field  $\vec{B}$  and current  $I$  flows between the two ends of the wedge. The Hall resistances  $R_{xy} = V_{xy}/I$  are measured at different thicknesses  $d$  to distinguish between surface and bulk Hall effects. For bulk conduction  $R_{xy}/B \propto 1/d$ , while  $R_{xy}/B$  is  $d$ -independent if surface conduction dominates. Although the side surfaces don't contribute to the Hall effect, we roughen the two surfaces on the thin and thick ends so they won't short-circuit the Hall voltage. We found the Hall voltage  $V_{xy}$  is linear with  $B$  (Fig. 1(a) inset) in all samples measured, bearing no signs of quantum oscillation <sup>16,17</sup> within our maximum magnetic field of 9 Tesla. Thus we can safely extract the value  $R_{xy}/B$  at various

temperatures  $T$ . Representative results in sample  $S1$  are plotted in Fig. 1(a) for  $d = 120, 270$  and  $320 \mu\text{m}$  respectively, showing clearly that while at high temperatures  $R_{xy}/B$  differ at different  $d$ , they converge to a same universal value of  $0.3 \Omega/T$  below 4 Kelvin, in consistence with surface conduction. Replotting the Hall resistance ratios  $R_{xy}(d_1)/R_{xy}(d_2)$  in Fig. 1(b), we found these ratios to be equal to  $d_2/d_1$  at high  $T$  and become unity at low  $T$ , proving the crossover from 3D to 2D Hall effects when  $T$  is lowered.

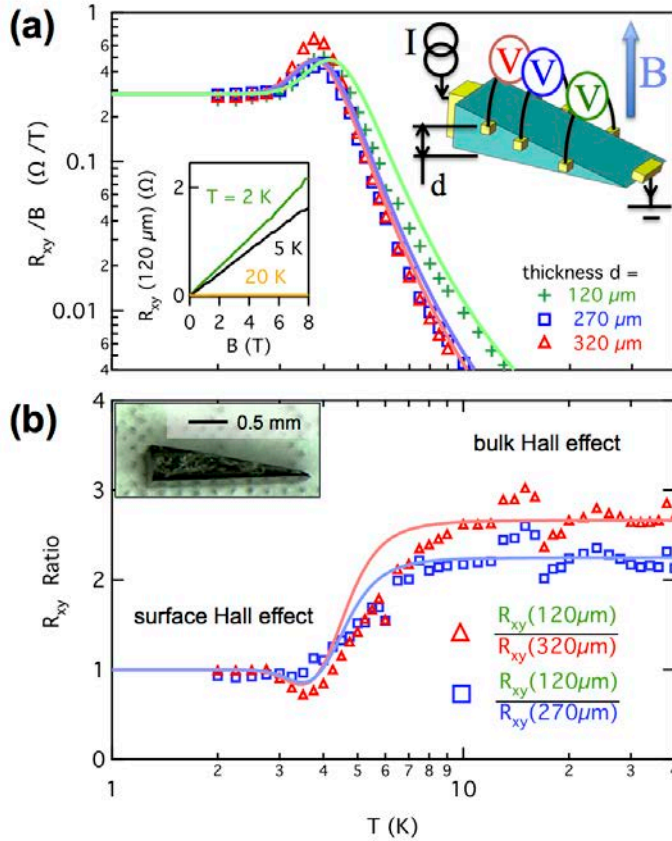


**Figure 1 | Surface Hall effect.** **a**, Markers, Hall resistances  $R_{xy}$  divided by magnetic field  $B$  versus temperature  $T$  at three different thicknesses  $d$  in a wedge shaped sample  $S1$ . Lines are simulations using a simplified model (see text). Left inset,  $R_{xy}$  versus  $B$  at various  $T$  for  $d = 120 \mu\text{m}$ . Right inset, measurement schematic. **b**, Markers, ratios between Hall resistances  $R_{xy}$  at different  $d$ . Lines are simulations. Inset, picture of sample  $S1$ .

In a TI where surface and bulk conductions are in parallel with each other, the Hall resistance depends not only on the carrier density but also on carrier mobility (Supplementary Information).

For a thin plate with top and bottom surfaces:

$$R_{xy} = \frac{B}{e} \frac{2n_S\mu_S^2 + d n_B \mu_B^2}{(2n_S\mu_S + d n_B\mu_B)^2}$$

And the longitudinal resistance  $R_{xx} = L / e w (2n_S\mu_S + d n_B\mu_B)$ , where  $n_S$  and  $n_B$  are surface and bulk carrier density,  $\mu_S$  and  $\mu_B$  are surface and bulk carrier mobility,  $e$  is electron charge,  $L$  is sample length and  $w$  is sample width. The bulk carrier density  $n_B$  should follow the standard activation law of a gapped insulator:  $n_B = n_B^0 \exp(-\Delta/k_B T)$ , where  $k_B$  is the Boltzmann's constant,  $n_B^0$  is a constant and  $\Delta$  is the bulk band gap. We found in all our samples the measured  $R_{xy}$  and  $R_{xx}$  fit well to the above "ideal" TI model by assuming  $\Delta = 38 K$ ,  $n_S = 1.1 \times 10^{15} cm^{-2}$ ,  $n_B^0 = 2 \times 10^{20} cm^{-3}$  and  $\mu_B = 500 cm^2/Vs$ . Only  $\mu_S$  varies between samples, which we will discuss further. We note the value of  $n_S$  approximately corresponds to two electrons per Sm atom on the surface. Using this simple model, we could reproduce the curious "peak" in  $R_{xy}/B$  at 4 K (solid lines in Fig. 1(a)), which lacks<sup>27</sup> a good explanation until now.

In QH<sup>8,9</sup> and QSH<sup>10,11</sup> states nonlocal transports have served as strong evidences<sup>6,7</sup> for the existence of the topological edge states that are one-dimensional analogues to the surface state in a TI. The highly metallic surface conduction in a TI would necessarily invalid Ohm's law and introduce large nonlocal voltages, which we have indeed found in SmB<sub>6</sub> samples. Fig. 2(a) shows a schematic of the nonlocal measurement in sample *S4*. Current  $I_{16}$  flows between current leads 1 and 6 at the centers on opposite faces of the crystal. Contacts 2 and 3 are located close to contact 1 for the detection of "local" voltage  $V_{23}$ . Contacts 4 and 5 are put near the sample edge

far away from the current leads to detect “nonlocal” voltage  $V_{45}$ . As shown in the inset in Fig. 2(b), in the case of bulk conduction, current will concentrate in the bulk near the current leads 1 and 6, resulting in negligibly small nonlocal voltage  $V_{45} \ll V_{23}$ . If surface conduction dominates, however, current will be forced to flow between contacts 1 and 6 via the surface, making  $V_{45}$  large. Fig. 2(a) shows as a function of temperature the measured  $V_{45}$  and  $V_{23}$  divided by  $I_{16}$ , both agreeing qualitatively with our finite element simulations (Supplementary Information) incorporating the aforementioned simple model. The ratio  $V_{45}/V_{23}$  is replotted in Fig. 2(b). At low temperature when surface conduction dominates the nonlocal voltage  $V_{45}$  becomes large and even surpasses the local voltage  $V_{23}$ . Above  $T = 5 K$  when bulk conduction dominates, the magnitude of  $V_{45}/V_{23}$  is very small. The negative sign of  $V_{45}/V_{23}$  is due to the small misalignment of contacts (Supplementary Information). The change of both magnitude and sign of  $V_{45}/V_{23}$  is reproduced by our simulation and highlights the distinction between high  $T$  bulk conduction and low  $T$  surface conduction.

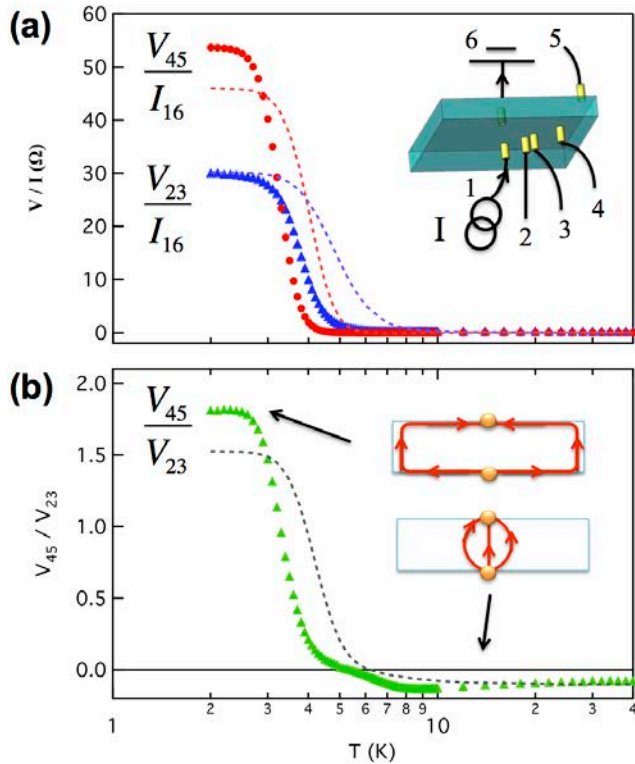


**Figure 2 | Nonlocal transport.** **a**, Markers, nonlocal resistance  $V_{45}/I_{16}$  and local resistance  $V_{23}/I_{16}$  versus temperature  $T$ . Dashed lines are finite element simulations. Inset is a schematic of the measurement configuration on sample S4. **b**, Ratio between nonlocal and local voltages  $V_{45}/V_{23}$  versus  $T$ . Dashed lines are finite element simulations. Inset, cartoons for current distribution in sample cross-section for surface and bulk dominated conduction.

An important aspect of TI: the topological protection of the surface state against time-reversal invariant perturbations was also explored in  $\text{SmB}_6$ . The robustness against perturbation distinguishes a topological surface state from “accidental” surface conduction<sup>4,5</sup>. We found the above surface Hall effect and nonlocal transport are recurrent phenomena in various samples and are robust to chemical and mechanical sample treatments. For example we have mechanically cut and scratched the surface of sample S10 (Fig. 3(a) inset) using a diamond knife and performed measurements before and after surface abrasion. We found the low temperature Hall resistance  $R_{xy}/B$  remain unchanged, indicating that the surface carrier density  $n_s$  was not affected by abrasion. The abrasion does reduce the surface mobility  $\mu_s$  though, as reflected by the height of

$R_{xy}/B$  “peak” at  $T = 4\text{ K}$  (Supplementary Information), presumably due to greatly enhanced geometric roughness. In a TI, surface carrier scattering is suppressed due to time-reversal symmetry, implying a ultra-high mobility useful for low power electronic devices<sup>4,5</sup>. However, surface absorbed molecules, though won’t destroy the metallic surface state, may alter the local energetics and degrade the intrinsic high mobility. We have tried different techniques to remove absorbed molecules. In particular, we show in Fig. 3(b) that the low temperature longitudinal resistance  $R_{xx}$  in sample *S14* was reduced by 1000 times after 12 hours of vacuum annealing. Since the Hall resistance was found largely unchanged, we conclude that the surface mobility  $\mu_S$  has been enhanced to  $72,000\text{ cm}^2/\text{Vs}$ , comparable to those found in graphene<sup>28</sup>.

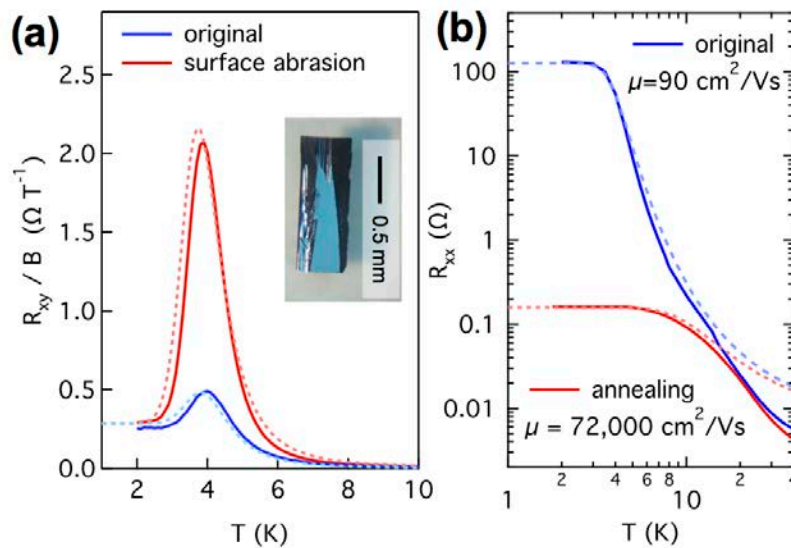


**Figure 3 | Robustness of the surface state.** **a**, Solid lines, Hall resistance  $R_{xy}$  divided by magnetic field  $B$  versus temperature  $T$ , before and after surface abrasion. Dashed lines are simulations assuming abrasion only reduces surface mobility  $\mu_S$ . Inset, picture of sample *S10* during abrasion. **b**, Solid lines, longitudinal resistance  $R_{xx}$  versus  $T$  in sample *S14* before and after vacuum annealing. Dashed lines are simulations assuming annealing only enhances  $\mu_S$  (to  $72,000\text{ cm}^2/\text{Vs}$ ).



The experimental identification of robust surface Hall effect and nonlocal transport serve as strong evidence that SmB<sub>6</sub> is an ideal topological insulator that has a protected highly metallic surface state surrounding a truly insulating bulk. The characterization of energetics of the surface state, however, awaits future investigations using energy and spin resolved techniques like ARPES<sup>2,3</sup> and STM<sup>12-14</sup>. Unlike weakly interacting TI materials, the strong electron correlation in SmB<sub>6</sub> could give rise to exotic emergent phases<sup>4,5</sup> with exciting new physics. For example it is known that SmB<sub>6</sub> is close to a ferromagnetic ground state<sup>27</sup>, pointing to the possibility of coexisting topological and magnetic orders. It would give rise to exotic electrodynamics<sup>4,5</sup> useful for low power spintronics. We reserve our results on this matter for a future publication.

*Note added:* During preparation of the manuscript, we became aware of a related work<sup>29</sup> in which evidence for surface conduction was provided in a SmB<sub>6</sub> sample with contacts arranged in a unique configuration.

## **METHODS SUMMARY**

High quality SmB<sub>6</sub> crystals were grown using the aluminium flux method. The surfaces of these crystals were carefully etched using hydrochloric acid and then cleaned using solvents to remove possible oxide layer or aluminium residues. These crystals are then inspected using X-ray analysis to make sure SmB<sub>6</sub> is the only content. Samples used in the experiments were made from these crystals either by mechanical cleaving or polishing using polishing films containing diamond particles. Gold and platinum wires are attached to the samples using micro spot welding and/or silver epoxy, with no discernable differences in measurements. Low frequency transport

measurements were carried out in helium cryostats using resistance bridge and standard low frequency (37 Hz) lock-in techniques with 5  $\mu A$  excitation currents.

1. Fu, L. & Kane, C. Topological insulators with inversion symmetry. *Phys Rev B* **76**, (2007).
2. Hsieh, D. *et al.* A topological Dirac insulator in a quantum spin Hall phase. *Nature* **452**, 970–974 (2008).
3. Chen, Y. L. *et al.* Experimental Realization of a Three-Dimensional Topological Insulator, Bi<sub>2</sub>Te<sub>3</sub>. *Science* **325**, 178–181 (2009).
4. Qi, X.-L. & Zhang, S.-C. Topological insulators and superconductors. *Rev Mod Phys* **83**, 1057–1110 (2011).
5. Hasan, M. & Kane, C. Colloquium: Topological insulators. *Rev Mod Phys* **82**, 3045–3067 (2010).
6. McEuen, P. *et al.* New resistivity for high-mobility quantum Hall conductors. *Phys Rev Lett* **64**, 2062–2065 (1990).
7. Roth, A. *et al.* Nonlocal Transport in the Quantum Spin Hall State. *Science* **325**, 294–297 (2009).
8. Klitzing, von, K., Dorga, G. & Pepper, M. New Method for High-Accuracy Determination of the Fine-Structure Constant Based on Quantized Hall Resistance. *Phys Rev Lett* **45**, 494–497 (1980).
9. Tsui, D. C., Stormer, H. L. & Gossard, A. C. Two-Dimensional Magnetotransport in the Extreme Quantum Limit. *Phys Rev Lett* **48**, 1559–1562 (1982).
10. Bernevig, B. A., Hughes, T. L. & Zhang, S. C. Quantum Spin Hall Effect and Topological Phase Transition in HgTe Quantum Wells. *Science* **314**, 1757–1761 (2006).
11. Koenig, M. *et al.* Quantum spin hall insulator state in HgTe quantum wells. *Science* **318**, 766–770 (2007).
12. Alpichshev, Z. *et al.* STM Imaging of Electronic Waves on the Surface of Bi<sub>2</sub>Te<sub>3</sub>: Topologically Protected Surface States and Hexagonal Warping Effects. *Phys Rev Lett* **104**, (2010).
13. Alpichshev, Z. *et al.* STM Imaging of Impurity Resonances on Bi<sub>2</sub>Se<sub>3</sub>. *Phys Rev Lett* **108**, (2012).
14. Roushan, P. *et al.* Topological surface states protected from backscattering by chiral spin texture. *Nature* **460**, 1106–1109 (2009).
15. Peng, H. *et al.* Aharonov-Bohm interference in topological insulator nanoribbons. *Nat Mater* **9**, 225–229 (2009).
16. Checkelsky, J., Hor, Y., Cava, R. & Ong, N. Bulk Band Gap and Surface State Conduction Observed in Voltage-Tuned Crystals of the Topological Insulator Bi<sub>2</sub>Se<sub>3</sub>. *Phys Rev Lett* **106**, 196801 (2011).
17. Analytis, J. G. *et al.* Two-dimensional surface state in the quantum limit of a topological insulator. *Nat Phys* **6**, 960–964 (2010).
18. Taskin, A. & Ando, Y. Quantum oscillations in a topological insulator Bi<sub>1-x</sub>Sb<sub>x</sub>. *Phys Rev B* **80**, 085303 (2009).
19. Kim, D. *et al.* Surface conduction of topological Dirac electrons in bulk insulating Bi<sub>2</sub>Se<sub>3</sub>. *Nat Phys* **8**, 460–464 (2012).

20. Nickerson, J. *et al.* Physical Properties of SmB<sub>6</sub>. *Phys Rev B* **3**, 2030–2042 (1971).
21. Barla, A. *et al.* High-Pressure Ground State of SmB<sub>6</sub>: Electronic Conduction and Long Range Magnetic Order. *Phys Rev Lett* **94**, (2005).
22. Derr, J. *et al.* From unconventional insulating behavior towards conventional magnetism in the intermediate-valence compound SmB<sub>6</sub>. *Phys Rev B* **77**, (2008).
23. Menth, A., Buehler, E. & Geballe, T. Magnetic and Semiconducting Properties of SmB<sub>6</sub>. *Phys Rev Lett* **22**, 295–297 (1969).
24. Miyazaki, H., Hajiri, T., Ito, T., Kunii, S. & Kimura, S.-I. Momentum-dependent hybridization gap and dispersive in-gap state of the Kondo semiconductor SmB<sub>6</sub>. *Phys Rev B* **86**, 075105 (2012).
25. Kim, D., Grant, T. & Fisk, Z. Limit Cycle and Anomalous Capacitance in the Kondo Insulator SmB<sub>6</sub>. *Phys Rev Lett* **109**, 096601 (2012).
26. Dzero, M., Sun, K., Galitski, V. & Coleman, P. Topological Kondo Insulators. *Phys Rev Lett* **104**, (2010).
27. Cooley, J., Aronson, M., Fisk, Z. & Canfield, P. SmB<sub>6</sub>: Kondo Insulator or Exotic Metal? *Phys Rev Lett* **74**, 1629–1632 (1995).
28. Geim, A. K. Graphene: Status and Prospects. *Science* **324**, 1530–1534 (2009).
29. Wolgast, S. *et al.* Discovery of the First True Three-Dimensional Topological Insulator: Samarium Hexaboride. *arXiv:1211.5104* (2012).

**Acknowledgements** We thank T.H. Geballe and A. Kapitulnik for useful discussions. This work was supported by UC Irvine CORCL Grant MIIG-2011-12-8 and NSF grant #DMR-0801253.

**Author Contributions** J.X and Z.F. conceived the project. D.J.K, T.G. and Z.F. grew the crystals. J.B., D.J.K., S.T. and J.X. fabricated the samples and performed the measurements. T.G. performed X-ray analysis of the crystals. S.T. and J.X. performed the simulations. All authors analysed the data and wrote the manuscript.

**Author Information** Correspondence and requests for materials should be addressed to J.X. ([xia.jing@uci.edu](mailto:xia.jing@uci.edu)).

## (Supplementary Information)

Since the measured Hall resistance  $R_{xy}$  is linear to magnetic field  $B$  up to our maximum field of 9 Tesla, the transport reported in the main text is still in the classical regime. Thus we use a simple classical model to fit our transport data. In this model, the surface of the sample is a metal with a surface carrier density  $n_S$  and surface carrier mobility  $\mu_S$ , both are temperature independent for simplicity. The bulk is a gapped insulator with an indirect activation gap  $\Delta$ . The bulk carrier density  $n_B$  thus follows activation law of an insulator:  $n_B = n_B^0 \exp(-\Delta/k_B T)$ , where  $k_B$  is the Boltzmann's constant and  $n_B^0$  is a constant. The bulk carrier mobility  $\mu_B$  is set to be temperature independent for simplicity.

To calculate longitudinal and Hall resistances, we consider a sample geometry shown in Fig. S1(a), where  $L$ ,  $w$   $d$  are the length, width and thickness of the sample respectively. The longitudinal resistance is just the parallel resistance of the surface and bulk channels:

$$R_{xx} = \frac{L}{e w (2n_S \mu_S + d n_B \mu_B)}$$

The factor 2 comes due to the fact there are bottom and top surfaces. The Hall resistance  $R_{xy}$  can be derived as the following: Consider the Hall measurement geometry in Fig. S1(a), where the surface carriers have an average velocity  $\vec{v}^S$ , and the bulk carriers have an average velocity  $\vec{v}^B$ . The electric field  $\vec{E}$  has components  $E_x$  and  $E_y$ . And  $R_{xy} = w E_y / I$ . When the current flow reaches equilibrium, the net current flow along the  $\vec{y}$  direction is zero:

$$2 n_S v_y^S + d n_B v_y^B = 0$$

The velocities  $v_y^S$  and  $v_y^B$  can be determined by noticing that they are the product of carrier mobility and the net Lorenz force.

$$v_y^S = \mu_S (E_y - v_x^S B) = \mu_S (E_y - \mu_S E_x B)$$

$$v_y^B = \mu_B (E_y - v_x^B B) = \mu_B (E_y - \mu_B E_x B)$$

Putting these three equations together, we have:

$$E_y = E_x B \frac{2n_S \mu_S^2 + d n_B \mu_B^2}{2n_S \mu_S + d n_B \mu_B}$$

Since  $E_x = I R_{xx}/L$ , we have:

$$E_x = \frac{I}{e w (2n_S \mu_S + d n_B \mu_B)}$$

Thus we can solve for  $E_y$ :

$$E_y = \frac{B I (2n_S \mu_S^2 + d n_B \mu_B^2)}{e w (2n_S \mu_S + d n_B \mu_B)^2}$$

The Hall resistance  $R_{xy}$  follows:

$$R_{xy} = w E_y / I = \frac{B (2n_S \mu_S^2 + d n_B \mu_B^2)}{e (2n_S \mu_S + d n_B \mu_B)^2}$$

Using these formulas for  $R_{xx}$  and  $R_{xy}$  we can plot in Fig. S1 (b) and (c) their temperature dependence in a sample with  $L = 1 \text{ mm}$ ,  $w = 300 \text{ } \mu\text{m}$ ,  $d = 200 \text{ } \mu\text{m}$ ,  $\Delta = 38 \text{ K}$ ,  $n_S = 1.1 \times 10^{15} \text{ cm}^{-2}$ ,  $\mu_S = 100 \text{ cm}^2/\text{Vs}$ ,  $n_B^0 = 2 \times 10^{20} \text{ cm}^{-3}$  and  $\mu_B = 500 \text{ cm}^2/\text{Vs}$ .

Using this simple model, we could also perform finite element simulations for the transport in more complicated geometries. Fig. S2 and Fig. S3 show the simulated surface potential profiles at  $300 \text{ K}$  and  $0 \text{ K}$  for the nonlocal transport experiment in a sample with thin plate geometry. The simulation curves in Fig. 3 in the main text are generated using this finite element simulation.

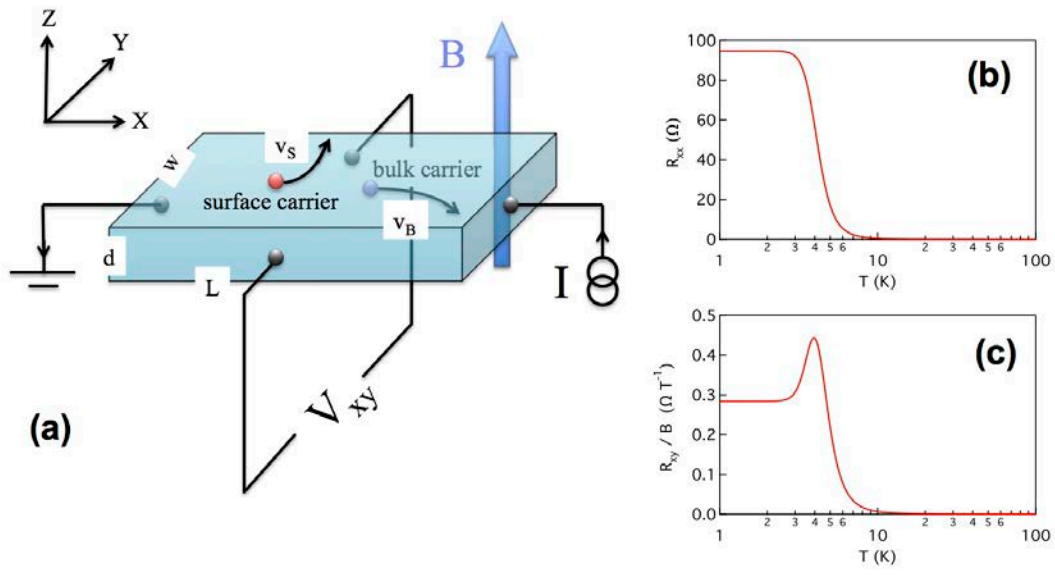


**Figure S1 | Simple Transport Model.** a, Schematic for Hall measurement when both bulk and surface conduction are present. b, c, Calculated  $R_{xy}$  and  $R_{xx}$  using this model (see text).

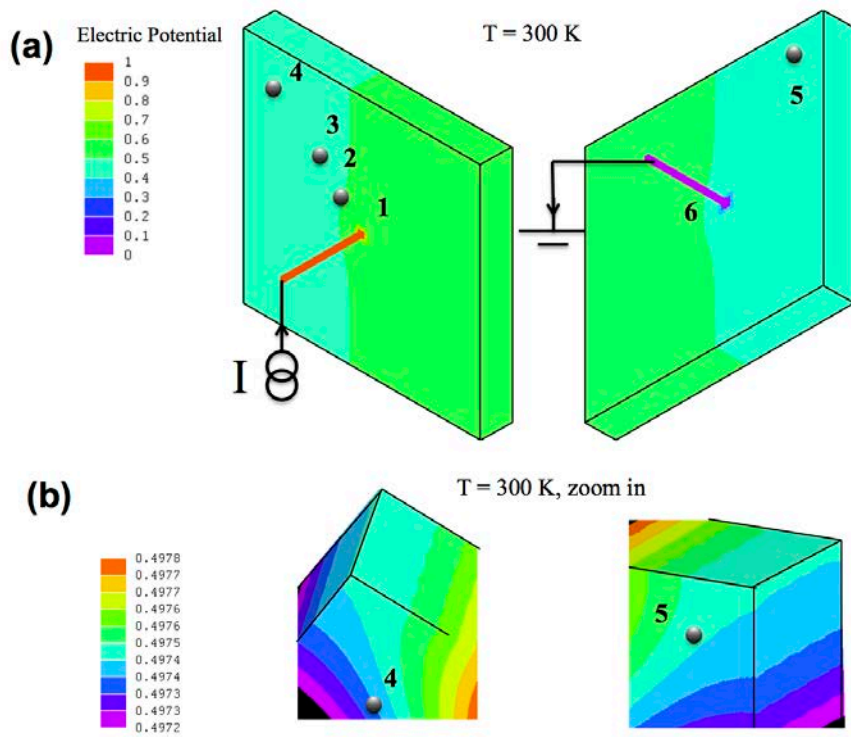


**Figure S2 | Simulation of Nonlocal Transport at 300 K.** a, Finite elements simulation of the surface potential profile in the nonlocal transport. As the conduction is dominated by the bulk,

the nonlocal voltage  $V_{45}$  is much smaller than  $V_{23}$ . **b**, Zoom in views for contact 4 and 5, showing  $V_{45}$  is a small negative value due to slight misalignment of contacts.

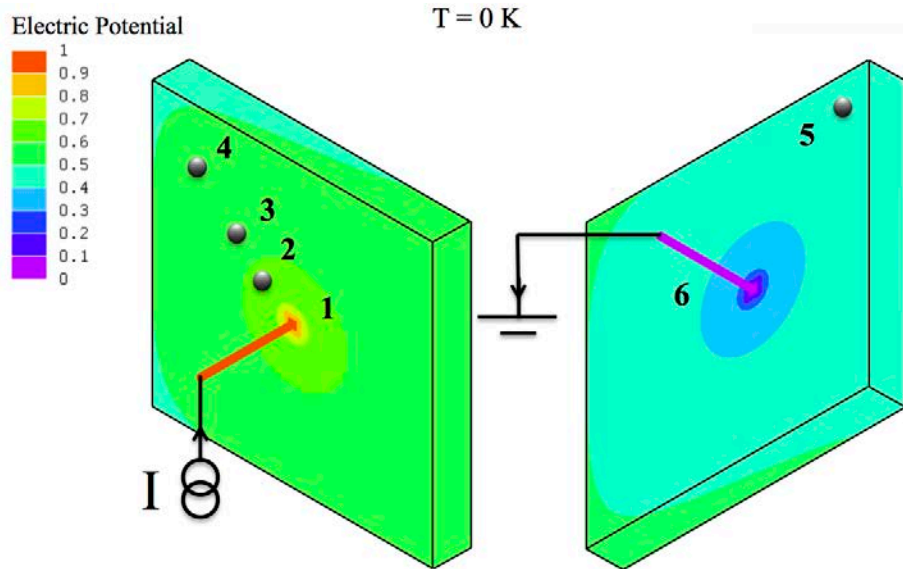


**Figure S3 | Simulation of Nonlocal Transport at 0 K.** **a**, Finite elements simulation of the surface potential profile in the nonlocal transport. Due to surface conduction, the nonlocal voltage  $V_{45}$  is large and is comparable to  $V_{23}$ .